Research Article | Vol. 27, No. 8 | 15 Apr 2019 | OPTICS EXPRESS 11174
Optics EXPRESS

Integrated polarizer based on 45° tilted gratings

MATTHEW T. POSNER,[1] NINA PODOLIAK,[1,2] DEVIN H. SMITH,[1,*] PAOLO L. MENNEA,[1] PETER HORAK,[1] CORIN B. E. GAWITH,[1] PETER G. R. SMITH,[1] AND JAMES C. GATES[1]

[1]*Optoelectronics Research Centre, University of Southampton, University Rd, Southampton, SO17 1BJ, UK*
[2]*Currently with Department of Mathematical Sciences, University of Southampton, University Rd, Southampton, SO17 1BJ, UK*
[*]*d.h.smith@soton.ac.uk*

Abstract: We report the first integrated implementation of a polarizer based on the use of 45° tilted gratings in planar waveguides. The waveguides and gratings are fabricated by direct UV writing in a hydrogenated germanium-doped silica-on-silicon chip. We experimentally demonstrate a polarization extinction ratio per unit length of 0.25 dB mm^{-1} with a modelled wavelength dependence smaller than 0.3 dB for a 20 mm device over the C band from 1530-1570 nm. We also present a novel numerical study and analytical description of the architecture that are in good agreement with each other and the experimental data.

1. Introduction

Photonic integrated polarizers are of interest in systems where the fidelity of the polarization state is crucial, such as coherent communications, quantum information processing and high-performance sensing. Integrated polarizers have been implemented in several monolithic platforms, including silicon [1], silicon-on-insulator [2] and indium phosphide [3]. These platforms present challenges for the integration of low insertion loss on-chip filters that are required for applications with stringent loss requirements, such as on-chip heralded single-photon generation [4]. Silica-based integrated circuits are attractive to overcome these limitations due to their intrinsically high coupling efficiency with fiber optics and low propagation loss. Many polarizing schemes make use of metallic layers or plasmonic coupling to induce preferential loss in one polarization [5, 6]; another possibility is active electrical polarization control through electrically tunable phase shifters and polarization rotators [7]. Each of these schemes has different merits and disadvantages, *e.g.* increased device complexity, complicated fabrication steps requiring stringent fabrication tolerances, or challenging low-loss integration into larger optical networks.

On the other hand, polarization control and management is well developed in optical fiber. Tilted UV-written Bragg gratings, wherein the grating planes are tilted with respect to the propagation axis, have been demonstrated as efficient polarizers [8, 9]. More specifically, gratings tilted at 45° fabricated by UV-irradiation of photosensitive silica fiber cores have achieved a polarization extinction ratio (PER) in excess of 40 dB [10], comparable to commercial components and with the added benefit of low insertion loss into fiber networks. The analogous implementation in a silica planar waveguide platform is therefore advantageous as it can be integrated into a larger and more complex photonic network on-chip with the potential for low-insertion loss [11]. One such fabrication approach is direct UV writing (DUW), a technique for the simultaneous fabrication of waveguides and gratings through a focused dual-beam UV-laser irradiation process in photosensitive silica chips [12].

To date there has been a small number of studies into tilted gratings in waveguide-based silica planar devices; those have been limited to the investigation of small-angle tilted gratings for spectroscopy and beam directing [13, 14], and theoretical considerations for 45° tilted gratings

#352964 https://doi.org/10.1364/OE.27.011174
Journal © 2019 Received 16 Jan 2019; revised 22 Feb 2019; accepted 22 Feb 2019; published 8 Apr 2019

Optics EXPRESS

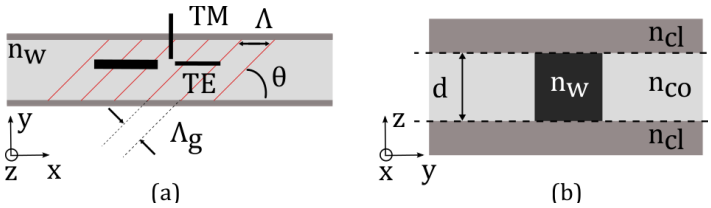

Fig. 1. (a) Schematic top view of the waveguide indicating tilted grating planes and polarization splitting effects. (b) Abstracted cross-section of the buried waveguide structure for modelling purposes. The transverse profile is nearly Gaussian in actual devices.

in waveguide ring-resonators [15]. The low refractive index contrast silica platform used here necessitates gratings of the order of millimeters in length, which are challenging to both fabricate and simulate; there is thus a gap in the literature in the modeling and fabrication for these planar devices.

We report, to our knowledge, the first proof-of-concept demonstration of an integrated waveguide polarizer based on tilted gratings, supported by a novel theoretical description of the architecture. This article will show the theoretical investigation, fabrication and testing of these structures—particularly their PER and spectral bandwidth response—to further understanding of the underlying behavior of these devices and offer routes to improve their performance.

2. Background and theory

A waveguide grating is a waveguide with a periodic modulation of the refractive index along its length. The grating-waveguide structure can be approximated as a succession of material interfaces with different refractive indices, as illustrated in Fig. 1(a). For low-contrast refractive index modulation ($\Delta n < 10^{-2}$), a beam incident upon a grating plane incurs negligible refraction and little Fresnel reflection for both the s (TE, E_z) and p (TM, E_y) polarizations. At a tilt of 45°, only s-polarized light is reflected by the grating, as the reflection coefficient for p-polarized light is identically zero due to Brewster's angle. This leads to the highest reflection difference between s- and p-polarization components, underlying the operation principle of the proposed integrated polarizer. This operation has been verified numerically [16] and analytically [17], and is in good agreement with experimental reports in the literature for UV-induced tilted gratings in silica fiber platforms. $\vec{k}$-vector theory can be used to design the normal grating period, Λ_g, as a function of the grating tilt angle, θ, with the grating period along the waveguide axis given by $\Lambda = \Lambda_g/\cos(\theta)$ [18]; the grating period at the resonant wavelength, $\lambda_\theta = 1550\,\text{nm}$, is thus $\Lambda = \lambda_\theta/2n_{\text{eff}}\cos(\theta)$, where n_{eff} is the effective refractive index of the waveguide mode. For the waveguides described here, $\Lambda_g \approx 750\,\text{nm}$. The grating period and tilt angle, which are used as the principal design parameters in this study, have been illustrated in Fig. 1(a).

Our waveguide implementation is based on the structure described in Fig. 1. A core layer of refractive index n_{co} and thickness d is sandwiched between under- and over-cladding layers with refractive indices n_{cl}; these claddings permit vertical confinement of a planar waveguide mode. The refractive index contrast between the planar core and claddings is assumed to support only a single transverse waveguide mode in the vertical (z) direction. We therefore limit modeling here to the transverse waveguide modes in the planar core layer, *i.e.* the $x-y$ plane of Fig. 1.

A planar architecture where a waveguide is defined in a photo-sensitive planar core layer by a focused Gaussian laser is thus the basis of our theoretical model. The refractive index profile of the waveguide, without the grating, n_{w}, is defined as

$$n_{\text{w}}(x, y) \equiv n_{\text{co}} + \Delta n \exp(-y^2/\sigma^2), \tag{1}$$

Optics EXPRESS

where Δn is the peak photo-induced refractive index contrast of the waveguide with respect to the core layer and σ is the width of the waveguide. With DUW, gratings are written interferometrically, simultaneously with the waveguide, yielding a grating refractive index profile [19]

$$\begin{aligned} n_g(x,y) &= n_w(x,y) + \Delta n_g \sin\left(2\pi \frac{x - y\tan(\theta)}{\Lambda}\right) \exp\left(-\frac{y^2}{\sigma^2}\right) \\ &= n_{co} + \left[\Delta n + \Delta n_g \sin\left(2\pi \frac{x - y\tan(\theta)}{\Lambda}\right)\right] \exp\left(-\frac{y^2}{\sigma^2}\right), \end{aligned} \tag{2}$$

where $\Delta n_g \leq \Delta n$ and is the index modulation of the sinusoidal grating. The average index along the waveguide remains constant both inside and outside the written grating period due to the simultaneous definition of the waveguide and grating.

To obtain an analytical expression for the PER, we used the beam tracing approach from [17]; the model was modified to account the overlap between the propagating mode and Gaussian transverse profile of the grating given in Eq. (2). The PER, $\Gamma(\lambda)$, of the 45° tilted grating was found to be

$$\Gamma(\lambda) = \Gamma_0 \exp\left[-\frac{2\pi^2\sigma^2 w_0^2}{\sigma^2 + w_0^2}\left(\frac{n_{eff}}{\lambda} - \frac{1}{\Lambda}\right)^2\right], \tag{3}$$

where w_0 is the mode field radius, n_{eff} is the mode effective index, and the maximal PER per unit length (in dB) at the resonant frequency, Γ_0/L, is

$$\frac{\Gamma_0}{L} = \frac{10\sqrt{2}\pi^{5/2}}{\ln(10)} \frac{\sigma^2 w_0}{\sigma^2 + w_0^2}\left(\frac{\Delta n_g}{2\Lambda n_{eff}}\right)^2, \tag{4}$$

which extends the work in [17] by considering the mode profile implied by Eq. (1).

We have used a finite-element modeling package (COMSOL Multiphysics) to simulate the integrated waveguide and grating structures described by Eqs. (1) and (2). The low refractive index contrast of DUW waveguides necessitates long interaction lengths for high efficiency grating polarizers; the computational requirements for modeling these gratings are beyond what is achievable without the use of high performance computer clusters. Therefore, we have numerically simulated gratings with shorter lengths (< 200 µm) and used these models to understand the physical mechanisms governing the grating structures and to verify the scalability of the analytical models. The field response of the device has been simulated for ten values of the refractive index modulation ($\Delta n_g = 5 \times 10^{-4} - 5 \times 10^{-3}$) and grating length ($L = 10 - 200$ µm), assuming a waveguide width $\sigma = 3$ µm and waveguide index contrast $\Delta n = 5 \times 10^{-3}$, which is consistent with previous results [20].

We have calculated the radiation loss, *i.e.* the scattering of light out of the guided waveguide mode, incurred by the grating as an s-polarized field propagates through the waveguide. Modeling confirms that in the devices of interest the p-polarized field is not reflected by the tilted gratings, and thus the radiation loss is equal to the PER, Γ. The simulated PER is shown as a function of grating length in Fig. 2(a) and refractive index modulation in Fig. 2(b). The PER of the polarizer is proportional to the grating length and has a quadratic dependence on the grating index modulation; this is in a good agreement with the analytical expression given by Eq. (3).

The grating-induced loss has also been modeled for ten wavelengths from 1500 − 1590 nm with tilted gratings of index contrast $\Delta n_g = 2 \times 10^{-3}$ and length $L = 50$ µm. The losses shown in Fig. 3 have been scaled to a grating length of 20 mm to predict the performance of the fabricated gratings. The wavelength dependence is lower than 0.3 dB over the C band (1530 − 1570 nm) and less than 0.8 dB over the entire range of wavelengths simulated. The large bandwidth is a consequence of the large angle of tilt of the gratings, and in agreement with theoretical studies of large-angle tilted gratings in fibers [21].

Optics EXPRESS

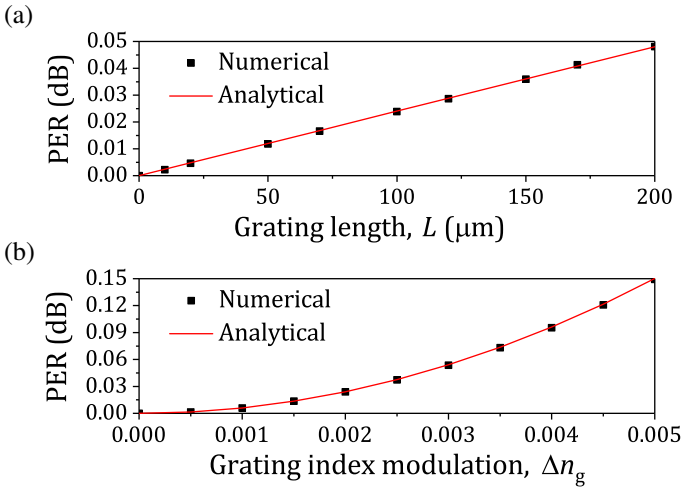

Fig. 2. PER calculated using numerical and analytical models for 45° tilted gratings with respect to (a) grating length and (b) grating refractive index modulation. The expected linear and quadratic dependencies respectively are clearly shown. For computational reasons, the gratings are quite short, leading to the low PER numbers shown.

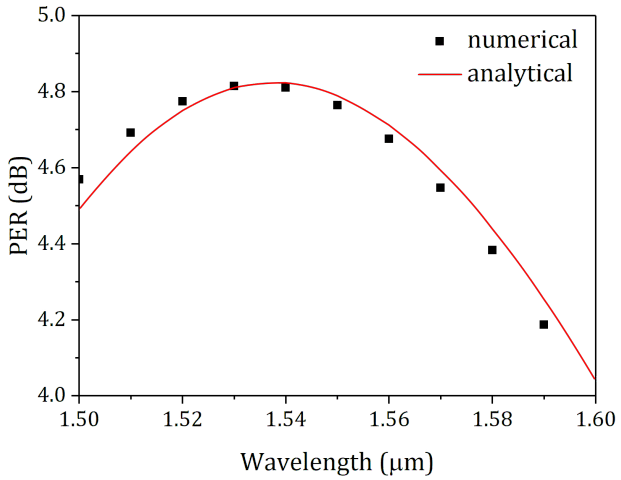

Fig. 3. Bandwidth performance of the devices, showing good agreement between numerics and the analytical calculation. The spectral offset is likely due to slight mismatch in n_{eff}, the effective index of the waveguide mode, between the two calculations.

3. Experimental results

The devices have been fabricated on a silicon wafer substrate with a thermal oxide of thickness 15 μm acting as the optical undercladding. A photosensitive germanoborosilicate planar core layer and an overcladding silica layer are deposited successively by flame hydrolysis deposition. The refractive index of the core has a higher refractive index than the overcladding, which is index-matched to the undercladding. Using two laser beams focused to a 6 μm spot and via electro-optic modulation of their relative phase, single-mode waveguides and gratings are defined simultaneously by DUW into the core layer. The crossing angle of the beams provides a fringe

Optics EXPRESS

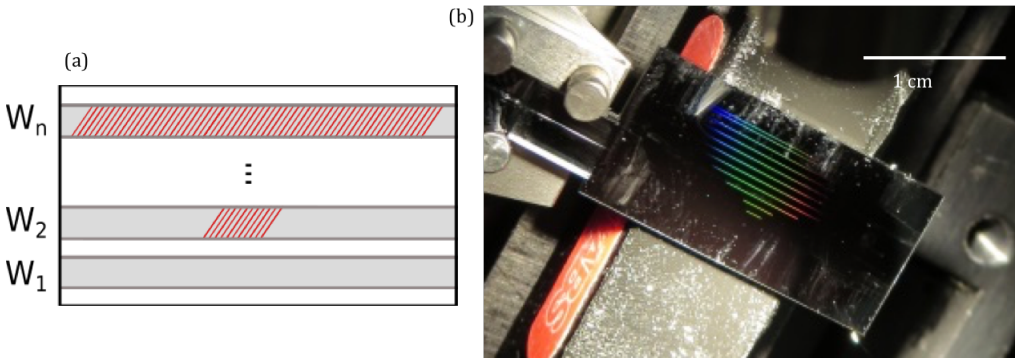

Fig. 4. (a) Schematic top view of the device under test with waveguides and gratings of increasing length. A total of 12 waveguides were fabricated. (b) Fabricated 20 mm silica-on-silicon chip highlighting the gratings of varying length visible as rainbow highlights, increasing in length toward the top of frame. Light is in-coupled from the left via fiber V-groove.

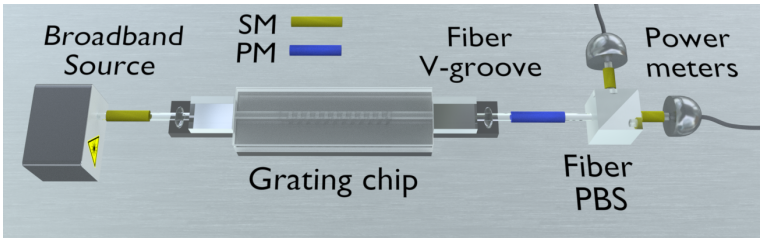

Fig. 5. On-chip tilted-grating polariser PER measurement setup; coupling in and out of the chip is via butt-coupled fiber V-groove assemblies.

pattern with a period of $\Lambda_g \approx 750$ nm. The samples are rotated by 45° relative to the fringe pattern during DUW to obtain 45° tilted gratings with $\Lambda \approx 1060$ nm. Twelve waveguides of length 20 mm, containing gratings 1 – 20 mm long, have been fabricated to verify the effect of grating length on PER and test the model, as shown in Fig. 4 (a). These include three waveguides with 20 mm gratings to assess reproducibility. The fabricated waveguides are shown in Fig. 4 (b); white-light illumination of the chip reveals the gratings. The waveguides are separated by a gap of 250 µm to prevent evanescent coupling between the waveguides.

The performance of the device was measured using an unpolarized erbium-doped fiber source (IPG Photonics) spanning the C band spectral range, coupled to the waveguides using a single-mode (SM) fiber mounted in a commercial V-groove assembly, as pictured in Fig. 4(b). The waveguide acts as the first polarizing element of the system and permits a self-referencing measurement of the PER. This setup removes the requirement for narrow-linewidth and highly polarized launch conditions and simplifies the launch scheme, with a typical insertion loss of 0.5 dB [11]. The signal is then collected by a polarizing-maintaining (PM) fiber mounted in a V-groove assembly. The alignment tolerance of the PM-fiber axes to the V-groove is specified to 2°, or a PER of 28 dB, and the tolerance of the V-groove alignment to the chip is comparable.

To characterize the PER, the collection PM fiber was connected to an integrated fiber polarizing beam splitter (PBS) (Thorlabs). Each output fiber of the PBS has been connected to two cross-referenced power meters (Exfo) to obtain power measurements, as illustrated in Fig. 5 (a). The PER was inferred from these power readings as the simple ratio of the power collected. The difference in propagation loss between TE and TM is negligible for DUW waveguides

Optics EXPRESS

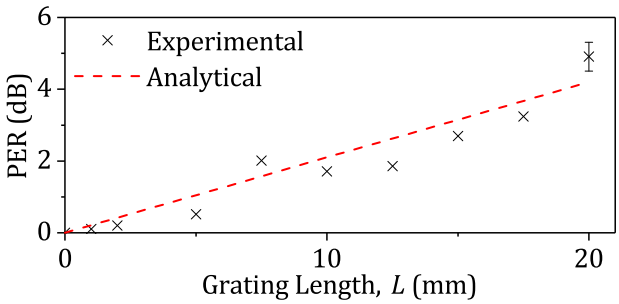

Fig. 6. Experimental PER with respect to grating length. Deviations from the straight line are assumed to represent variation in fabrication, likely due to outgassing of hydrogen. The error bar at 20 mm represents the standard error of the three devices made at that length.

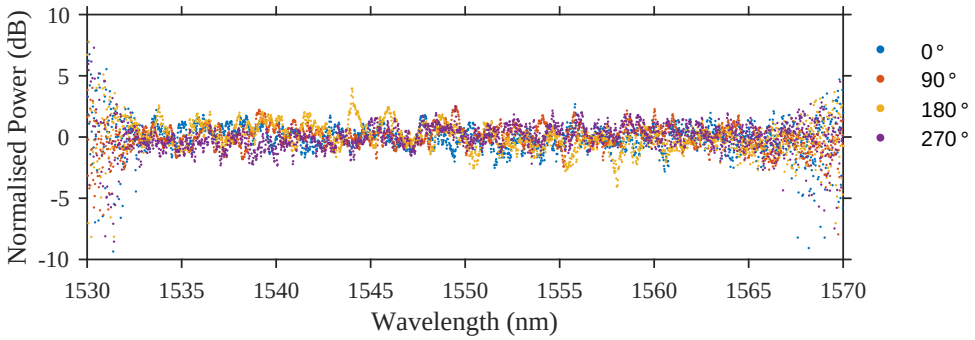

Fig. 7. Spectral response of the device at four angles, normalised to the same average power. The noise at the edges is due to the finite bandwidth of the light source used, causing the signal to reach the noise floor.

(< 0.001 dB mm^{-1}) [22], thus the power ratios have been normalized with respect to a waveguide without a grating. The PER for the fabricated gratings are presented along with a linear fit in Fig. 6. The PER per unit length, Γ_0/L, is measured to be 0.25 dB mm^{-1}. The maximum PER, for 20 mm devices at 1550 nm is (4.9 ± 0.4) dB; the error stated is the standard deviation of three nominally identical 20 mm gratings. The deviation of the data from the line of best fit may be due to variation in the waveguide n_{eff} during the fabrication process. The grating refractive index modulation has been inferred from Eq. 3 as $\Delta n_g = 3.2 \times 10^{-3}$ via grating interrogation of DUW waveguides; this value is comparable to prior measurements of Δn_g [12]. Previous work suggests that a increasing the writing fluence should increase both Δn and, proportionally, Δn_g [12], and given that this parameter increases performance quadratically, Γ_0/L of 0.5 dB mm^{-1} should be feasible. With chip lengths up to approximately 60 mm fabricable using existing methods to correct for stress-induced curvature, a total PER of 30 dB should be achievable while keeping the propagation loss below 1.2 dB. Coupling PM fiber via V-groove arrays to this device then matches the specified performance characteristics of the V-groove with that of the grating polarizer.

The fiber PBS used above had limited loss bandwidth which made it unsuitable for measuring the spectral response of the fabricated devices. The experimental setup was thus adapted to incorporate a bulk Glan-Thomson polarizer (PER > 50 dB) mounted in a rotation holder. The output PM fiber was mounted in a fiber holder and imaged through a microscope objective. The signal was transmitted through the polarizer and coupled into a multi-mode (MM) fiber

Optics EXPRESS

that was connected to an optical spectrum analyzer for spectral characterization. The recorded spectra, recorded at four angles both parallel- and cross-polarized, were somewhat noisy due to limited signal at the detector, but showed very little spectral dependence, as shown in Fig. 7. A simple standard deviation of the signals was in the $0.2 - 0.5$ db range across the C band, within the bounds set by theory (see Fig. 3); unfortunately, the expected spectral response from the theoretical work is dominated by statistical noise.

4. Conclusion

In conclusion, this article has described the first theoretical and experimental study demonstrating a proof-of-principle implementation of 45° tilted gratings in UV-written silica-on-silicon waveguides. Whilst the PER of preliminary devices is limited ($0.25\,\mathrm{dB\,mm^{-1}}$) they offer a broadband spectral response spanning the C band, and optimization of the refractive index modulation scheme should yield a quadratic improvement of in device performance according to our model. The large bandwidth relaxes the waveguide uniformity requirements, as is normally needed for waveguides containing Bragg gratings. The fabrication techniques could also therefore be applied for use with other integrated buried planar waveguide circuits, such as germanium-doped silica channel waveguides. The structures may be incorporated as building blocks or integrated on chip alongside other integrated network functions such as interferometers and couplers. This type of integrated waveguide-based tilted grating offers a polarization filtering capability for many applications in sensing, telecommunications and quantum information processing.

Funding

Engineering and Physical Sciences Research Council (EPSRC), UK (EP/M013243/1, EP/M013294/1, EP/M024539/1, EP/K034480/1, 1375564).

Acknowledgments

All data supporting this study are openly available from the University of Southampton repository at https://doi.org/10.5258/SOTON/D0352.

References

1. D. Dai, J. Bauters, and J. E. Bowers, "Passive technologies for future large-scale photonic integrated circuits on silicon: polarization handling, light non-reciprocity and loss reduction," Light. Sci. Appl. **1**, e1 (2012).
2. D. Dai, Z. Wang, N. Julian, and J. E. Bowers, "Compact broadband polarizer based on shallowly-etched silicon-on-insulator ridge optical waveguides," Opt. Express **18**, 27404–27415 (2010).
3. L. M. Augustin, R. Hanfoug, J. J. G. M. van der Tol, W. J. M. de Laat, and M. K. Smit, "A compact integrated polarization splitter/converter in InGaAsP–InP," IEEE Photonics Technol. Lett. **19**, 1286–1288 (2007).
4. J. B. Spring, P. L. Mennea, B. J. Metcalf, P. C. Humphreys, J. C. Gates, H. L. Rogers, C. Söller, B. J. Smith, W. S. Kolthammer, P. G. R. Smith, and I. A. Walmsley, "Chip-based array of near-identical, pure, heralded single-photon sources," Optica **4**, 90–96 (2017).
5. L. Zhou and W. Liu, "Broadband polarizing beam splitter with an embedded metal-wire nanograting," Opt. Lett. **30**, 1434–1436 (2005).
6. B. Shen, P. Wang, R. Polson, and R. Menon, "An integrated-nanophotonics polarization beamsplitter with 2.4×2.4 μm^2 footprint," Nat. Photonics **9**, 378–382 (2015).
7. J. D. Sarmiento-Merenguel, R. Halir, X. L. Roux, C. Alonso-Ramos, L. Vivien, P. Cheben, E. Durán-Valdeiglesias, I. Molina-Fernández, D. Marris-Morini, D.-X. Xu, J. H. Schmid, S. Janz, and A. Ortega-Moñux, "Demonstration of integrated polarization control with a 40 dB range in extinction ratio," Optica **2**, 1019–1023 (2015).
8. P. Westbrook, T. Strasser, and T. Erdogan, "In-line polarimeter using blazed fiber gratings," IEEE Photonics Technol. Lett. **12**, 1352–1354 (2000).
9. S. Mihailov, R. Walker, T. Stocki, and D. Johnson, "Fabrication of tilted fibre-grating polarisation-dependent loss equaliser," Electron. Lett. **37**, 284–286 (2001).
10. Z. Yan, C. Mou, K. Zhou, X. Chen, and L. Zhang, "UV-inscription, polarization-dependant loss characteristics and applications of 45° tilted fiber gratings," J. Light. Technol. **29**, 2715–2724 (2011).

Optics EXPRESS

11. P. L. Mennea, W. R. Clements, D. H. Smith, J. C. Gates, B. J. Metcalf, R. H. S. Bannerman, R. Burgwal, J. J. Renema, W. S. Kolthammer, I. A. Walmsley, and P. G. R. Smith, "Modular linear optical circuits," Optica **5**, 1087–1090 (2018).
12. C. Sima, J. C. Gates, H. L. Rogers, P. L. Mennea, C. Holmes, M. N. Zervas, and P. G. R. Smith, "Ultra-wide detuning planar Bragg grating fabrication technique based on direct UV grating writing with electro-optic phase modulation," Opt. Express **21**, 15747–15754 (2013).
13. C. K. Madsen, J. Wagener, T. A. Strasser, D. Muehlner, M. A. Milbrodt, E. J. Laskowski, and J. Demarco, "Planar waveguide optical spectrum analyzer using a UV-induced grating," IEEE J. Sel. Top. Quantum Electron. **4**, 925–929 (1998).
14. C. Holmes, L. G. Carpenter, H. L. Rogers, I. J. G. Sparrow, J. C. Gates, and P. G. R. Smith, "Planar waveguide tilted Bragg grating refractometer fabricated through physical micromachining and direct UV writing," Opt. Express **19**, 12462–12468 (2011).
15. H. Ma, J. Zhang, Z. Chen, and Z. Jin, "Tilted waveguide gratings and implications for optical waveguide-ring resonator," J. Light. Technol. **33**, 4176–4183 (2015).
16. Y. Li, M. Froggatt, and T. Erdogan, "Volume current method for analysis of tilted fiber," J. Light. Technol. **19**, 1580–1591 (2001).
17. T. Yoshino, "Theoretical analysis of a tilted fiber grating polarizer by the beam tracing approach," J. Opt. Soc. Am. B **29**, 2478–2483 (2012).
18. G. Nemova, J. Chauve, and R. Kashyap, "Design of sidetap fiber Bragg grating filters," Opt. Commun. **259**, 649–654 (2006).
19. R. Kashyap, "Chapter 4 - Theory of fiber Bragg gratings," in *Fiber Bragg Gratings,* (Academic, 1999), pp. 119–194.
20. C. Sima, J. C. Gates, C. Holmes, P. L. Mennea, M. N. Zervas, and P. G. R. Smith, "Terahertz bandwidth photonic Hilbert transformers based on synthesized planar Bragg grating fabrication," Opt. Lett. **38**, 3448–3451 (2013).
21. T. Erdogan, "Fiber grating spectra," J. Light. Technol. **15**, 1277–1294 (1997).
22. H. L. Rogers, S. Ambran, C. Holmes, J. C. Gates, and P. G. R. Smith, "In situ loss measurement of direct UV-written waveguides using integrated Bragg gratings," Opt. Lett. **35**, 2849–2851 (2010).